Research Article | Vol. 26, No. 10 | 14 May 2018 | OPTICS EXPRESS A433
Optics EXPRESS

Development of a portable cavity ring down spectroscopy instrument for simultaneous, in situ measurement of NO_3 and N_2O_5

ZHIYAN LI,[1,2] RENZHI HU,[1,5] PINHUA XIE,[1,3,6] HAO CHEN,[1] SHENGYANG WU,[1] FENGYANG WANG,[1] YIHUI WANG,[1] LIUYI LING,[3] JIANGUO LIU,[1] AND WENQING LIU[1]

[1]*Key Lab. of Environmental Optics and Technology, Anhui Institute of Optics and Fine Mechanics, Chinese Academy of Sciences, Hefei, 230031, Anhui, China*
[2]*Science Island Branch of Graduate School, University of Science and Technology of China, Hefei, 230026, Anhui, China*
[3]*CAS Center for Excellence in Regional Atmospheric Environment, Institute of Urban Environment, Chinese Academy of Sciences, Xiamen, 361000, Fujian, China*
[4]*School of Electrical and Information Engineering, Anhui University of science & technology, Huainan, 232001, Anhui, China*
[5]*rzhu@aiofm.ac.cn*
[6]*phxie@aiofm.ac.cn*

Abstract: An inexpensive, compact instrument for sensitive measurement of nocturnal nitrogen oxides NO_3 and N_2O_5 in ambient air at high time resolution has been described. The instrument measures NO_3 and N_2O_5 which is converted into the NO_3 radical through thermal decomposition by optical extinction using a diode laser at 662.08 nm in two separate detection channels. The minimum detection limits (1σ) for the NO_3 radical and N_2O_5 are estimated to be 2.3 pptv and 3.1 pptv in an average time of 2.5 s, with the accessible effective absorption path length generally exceeding 30 km, which is sufficient for quantifying NO_3 radical and N_2O_5 concentrations under moderately polluted conditions. The total uncertainties of the NO_3 and N_2O_5 measurements are 8% and 15% respectively, which are mainly dominated by the uncertainty of NO_3 across section calculated for 353 K in this system. In addition, the dependence of the instrument's sensitivity and accuracy on a variety of conditions was presented in winter of 2016 and in summer of 2017 during two China-UK joint campaigns. Distinct N_2O_5 vertical profiles were observed at night in winter. The equilibrium among observed NO_2, NO_3 and N_2O_5 based on the equilibrium constants during summer time also provides confirmation of the measurement accuracy of the instrument.

OCIS codes: (010.1120) Air pollution monitoring; (120.4640) Optical instruments; (300.6550) Spectroscopy, visible.

References and links

1. R. P. Wayne, I. Barnes, P. Biggs, J. P. Burrows, C. E. Canosamas, J. Hjorth, G. Lebras, G. K. Moortgat, D. Perner, G. Poulet, G. Restelli, and H. Sidebottom, "The nitrate radical: Physics, chemistry, and the atmosphere," Atmos. Environ. **25**(1), 1–203 (1991).
2. S. S. Brown and J. Stutz, "Nighttime radical observations and chemistry," Chem. Soc. Rev. **41**(19), 6405–6447 (2012).
3. W. L. Chang, P. V. Bhave, S. S. Brown, N. Riemer, J. Stutz, and D. Dabdub, "Heterogeneous Atmospheric Chemistry, Ambient Measurements, and Model Calculations of N_2O_5: A Review," Aerosol Sci. Technol. **45**(6), 665–695 (2011).
4. S. S. Brown, J. E. Dibb, H. Stark, M. Aldener, M. Vozella, S. Whitlow, E. J. Williams, B. M. Lerner, R. Jakoubek, A. M. Middlebrook, J. A. DeGouw, C. Warneke, P. D. Goldan, W. C. Kuster, W. M. Angevine, D. T. Sueper, P. K. Quinn, T. S. Bates, J. F. Meagher, F. C. Fehsenfeld, and A. R. Ravishankara, "Nighttime removal of NO_x in the summer marine boundary layer," Geophys. Res. Lett. **31**(7), 1–5 (2004).
5. F. J. Dentener and P. J. Crutzen, "reaction of N_2O_5 on tropospheric aerosols-impact on the global distributions of NO_x, O_3 and OH," J. Geophys. Res. Atmos. **98**(D4), 7149–7163 (1993).

#319620 https://doi.org/10.1364/OE.26.00A433
Journal © 2018 Received 16 Jan 2018; revised 21 Mar 2018; accepted 21 Mar 2018; published 3 Apr 2018

6. R. C. Sullivan, S. A. Guazzotti, D. A. Sodeman, and K. A. Prather, "Direct observations of the atmospheric processing of Asian mineral dust," Atmos. Chem. Phys. **7**(5), 1213–1236 (2007).
7. S. S. Brown, H. Stark, and A. R. Ravishankara, "Applicability of the steady state approximation to the interpretation of atmospheric observations of NO_3 and N_2O_5," J. Geophys. Res. **108**(D17), 4539 (2003).
8. K. M. Emmerson and N. Carslaw, "Night-time radical chemistry during the TORCH campaign," Atmos. Environ. **43**(20), 3220–3226 (2009).
9. L. Xue, R. Gu, T. Wang, X. Wang, S. Saunders, D. Blake, P. K. K. Louie, C. W. Y. Luk, I. Simpson, Z. Xu, Z. Wang, Y. Gao, S. Lee, A. Mellouki, and W. Wang, "Oxidative capacity and radical chemistry in the polluted atmosphere of Hong Kong and Pearl River Delta region: analysis of a severe photochemical smog episode," Atmos. Chem. Phys. **16**(15), 9891–9903 (2016).
10. S. S. Brown, H. An, M. Lee, J.-H. Park, S.-D. Lee, D. L. Fibiger, E. E. McDuffie, W. P. Dubé, N. L. Wagner, and K.-E. Min, "Cavity enhanced spectroscopy for measurement of nitrogen oxides in the Anthropocene: results from the Seoul tower during MAPS 2015," Faraday Discuss. **200**, 529–557 (2017).
11. T. Wang, Y. J. Tham, L. Xue, Q. Li, Q. Zha, Z. Wang, S. C. N. Poon, W. P. Dubé, D. R. Blake, P. K. K. Louie, C. W. Y. Luk, W. Tsui, and S. S. Brown, "Nighttime chemistry at a high altitude site above Hong Kong," J. Geophys. Res. Atmos. **121**(5), 2457–2475 (2016).
12. N. L. Ng, S. S. Brown, A. T. Archibald, E. Atlas, R. C. Cohen, J. N. Crowley, D. A. Day, N. M. Donahue, J. L. Fry, H. Fuchs, R. J. Griffin, M. I. Guzman, H. Herrmann, A. Hodzic, Y. Iinuma, J. L. Jimenez, A. Kiendler-Scharr, B. H. Lee, D. J. Luecken, J. Mao, R. McLaren, A. Mutzel, H. D. Osthoff, B. Ouyang, B. Picquet-Varrault, U. Platt, H. O. T. Pye, Y. Rudich, R. H. Schwantes, M. Shiraiwa, J. Stutz, J. A. Thornton, A. Tilgner, B. J. Williams, and R. A. Zaveri, "Nitrate radicals and biogenic volatile organic compounds: oxidation, mechanisms, and organic aerosol," Atmos. Chem. Phys. **17**(3), 2103–2162 (2017).
13. B. R. Ayres, H. M. Allen, D. C. Draper, S. S. Brown, R. J. Wild, J. L. Jimenez, D. A. Day, P. C. Campuzano-Jost, W. Hu, J. de Gouw, A. Koss, R. C. Cohen, K. C. Duffey, P. Romer, K. Baumann, E. Edgerton, S. Takahama, J. A. Thornton, B. H. Lee, F. D. Lopez-Hilfiker, C. Mohr, P. O. Wennberg, T. B. Nguyen, A. Teng, A. H. Goldstein, K. Olson, and J. L. Fry, "Organic nitrate aerosol formation via NO_3 + biogenic volatile organic compounds in the southeastern United States," Atmos. Chem. Phys. **15**(23), 13377–13392 (2015).
14. . L. Fry, A. Kiendler-Scharr, A. W. Rollins, P. J. Wooldridge, S. S. Brown, H. Fuchs, W. Dubé, A. Mensah, M. dal Maso, R. Tillmann, H.-P. Dorn, T. Brauers, and R. C. Cohen, "Organic nitrate and secondary organic aerosol yield from NO_3 oxidation of beta-pinene evaluated using a gas-phase kinetics/aerosol partitioning model," Atmos. Chem. Phys. **9**(4), 1431–1449 (2009).
15. S. S. Brown, J. A. Degouw, C. Warneke, T. B. Ryerson, W. P. Dubé, E. Atlas, R. J. Weber, R. E. Peltier, J. A. Neuman, J. M. Roberts, A. Swanson, F. Flocke, S. A. McKeen, J. Brioude, R. Sommariva, M. Trainer, F. C. Fehsenfeld, and A. R. Ravishankara, "Nocturnal isoprene oxidation over the Northeast United States in summer and its impact on reactive nitrogen partitioning and secondary organic aerosol," Atmos. Chem. Phys. **9**(9), 3027–3042 (2009).
16. N. Sobanski, M. J. Tang, J. Thieser, G. Schuster, D. Pohler, H. Fischer, W. Song, C. Sauvage, J. Williams, J. Fachinger, F. Berkes, P. Hoor, U. Platt, J. Lelieveld, and J. N. Crowley, "Chemical and meteorological influences on the lifetime of NO_3 at a semi-rural mountain site during PARADE," Atmos. Chem. Phys. **16**(8), 4867–4883 (2016).
17. J. N. Crowley, J. Thieser, M. J. Tang, G. Schuster, H. Bozem, Z. H. Beygi, H. Fischer, J. M. Diesch, F. Drewnick, S. Borrmann, W. Song, N. Yassaa, J. Williams, D. Pöhler, U. Platt, and J. Lelieveld, "Variable lifetimes and loss mechanisms for NO_3 and N_2O_5 during the DOMINO campaign: contrasts between marine, urban and continental air," Atmos. Chem. Phys. **11**(21), 10853–10870 (2011).
18. S. S. Brown, H. Stark, T. B. Ryerson, E. J. Williams, D. K. Nicks, Jr., M. Trainer, F. C. Fehsenfeld, and A. R. Ravishankara, "Nitrogen oxides in the nocturnal boundary layer: Simultaneous in situ measurements of NO_3, N_2O_5, NO_2, NO, and O_3," J. Geophys. Res. Atmos. **108**(D9), 11 (2003).
19. R. McLaren, P. Wojtal, D. Majonis, J. McCourt, J. D. Halla, and J. Brook, "NO_3 radical measurements in a polluted marine environment: links to ozone formation," Atmos. Chem. Phys. **10**(9), 4187–4206 (2010).
20. J. D. Ayers and W. R. Simpson, "Measurements of N_2O_5 near Fairbanks, Alaska," J. Geophys. Res. Atmos. **111**(D14), D14309 (2006).
21. R. McLaren, R. A. Salmon, J. Liggio, K. L. Hayden, K. G. Anlauf, and W. R. Leaitch, "Nighttime chemistry at a rural site in the Lower Fraser Valley," Atmos. Environ. **38**(34), 5837–5848 (2004).
22. J. Matsumoto, K. Imagawa, H. Imai, N. Kosugi, M. Ideguchi, S. Kato, and Y. Kajii, "Nocturnal sink of NOx via NO_3 and N_2O_5 in the outflow from a source area in Japan," Atmos. Environ. **40**(33), 6294–6302 (2006).
23. J. N. Crowley, G. Schuster, N. Pouvesle, U. Parchatka, H. Fischer, B. Bonn, H. Bingemer, and J. Lelieveld, "Nocturnal nitrogen oxides at a rural mountain-site in south-western Germany," Atmos. Chem. Phys. **10**(6), 2795–2812 (2010).
24. T. Nakayama, T. Ide, F. Taketani, M. Kawai, K. Takahashi, and Y. Matsumi, "Nighttime measurements of ambient N_2O_5, NO_2, NO and O_3 in a sub-urban area, Toyokawa, Japan," Atmos. Environ. **42**(9), 1995–2006 (2008).
25. S. S. Brown, W. P. Dubé, J. Peischl, T. B. Ryerson, E. Atlas, C. Warneke, J. A. deGouw, S. L. Hekkert, C. A. Brock, F. Flocke, M. Trainer, D. D. Parrish, F. C. Feshenfeld, and A. R. Ravishankara, "Budgets for nocturnal VOC oxidation by nitrate radicals aloft during the 2006 Texas Air Quality Study," J. Geophys. Res. Atmos. **116**(D24), D24305 (2011).

Optics EXPRESS

26. S. S. Brown, W. P. Dube, R. Bahreini, A. M. Middlebrook, C. A. Brock, C. Warneke, J. A. deGouw, R. A. Washenfelder, E. Atlas, J. Peischl, T. B. Ryerson, J. S. Holloway, J. P. Schwarz, R. Spackman, M. Trainer, D. D. Parrish, F. C. Fehshenfeld, and A. R. Ravishankara, "Biogenic VOC oxidation and organic aerosol formation in an urban nocturnal boundary layer: aircraft vertical profiles in Houston, TX," Atmos. Chem. Phys. **13**(22), 11317–11337 (2013).
27. A. K. Benton, J. M. Langridge, S. M. Ball, W. J. Bloss, M. Dall'Osto, E. Nemitz, R. M. Harrison, and R. L. Jones, "Night-time chemistry above London: measurements of NO_3 and N_2O_5 from the BT Tower," Atmos. Chem. Phys. **10**(20), 9781–9795 (2010).
28. N. L. Wagner, T. P. Riedel, C. J. Young, R. Bahreini, C. A. Brock, W. P. Dubé, S. Kim, A. M. Middlebrook, F. Ozturk, J. M. Roberts, R. Russo, B. Sive, R. Swarthout, J. A. Thornton, T. C. VandenBoer, Y. Zhou, and S. S. Brown, "N_2O_5 uptake coefficients and nocturnal NO_2 removal rates determined from ambient wintertime measurements," J. Geophys. Res. Atmos. **118**(16), 9331–9350 (2013).
29. S. S. Brown, W. P. Dube, H. D. Osthoff, J. Stutz, T. B. Ryerson, A. G. Wollny, C. A. Brock, C. Warneke, J. A. De Gouw, E. Atlas, J. A. Neuman, J. S. Holloway, B. M. Lerner, E. J. Williams, W. C. Kuster, P. D. Goldan, W. M. Angevine, M. Trainer, F. C. Fehsenfeld, and A. R. Ravishankara, "Vertical profiles in NO_3 and N_2O_5 measured from an aircraft: Results from the NOAA P-3 and surface platforms during the New England Air Quality Study 2004," J. Geophys. Res. Atmos. **112**(D22), D22304 (2007).
30. J. Stutz, K. W. Wong, L. Lawrence, L. Ziemba, J. H. Flynn, B. Rappenglück, and B. Lefer, "Nocturnal NO_3 radical chemistry in Houston, TX," Atmos. Environ. **44**(33), 4099–4106 (2010).
31. C. Tsai, C. Wong, S. Hurlock, O. Pikelnaya, L. H. Mielke, H. D. Osthoff, J. H. Flynn, C. Haman, B. Lefer, J. Gilman, J. deGouw, and J. Stutz, "Nocturnal loss of NOx during the 2010 CalNex-LA study in the Los Angeles Basin," J. Geophys. Res. Atmos. **119**(22), 13004–13025 (2014).
32. H. Wang, J. Chen, and K. Lu, "Development of a portable cavity-enhanced absorption spectrometer for the measurement of ambient NO_3 and N_2O_5: experimental setup, lab characterizations, and field applications in a polluted urban environment," Atmos. Meas. Tech. **10**(4), 1465–1479 (2017).
33. S. Wang, C. Shi, B. Zhou, H. Zhao, Z. Wang, S. Yang, and L. Chen, "Observation of NO_3 radicals over Shanghai, China," Atmos. Environ. **70**, 401–409 (2013).
34. H. Wang, K. Lu, X. Chen, Q. Zhu, Q. Chen, S. Guo, M. Jiang, X. Li, D. Shang, Z. Tan, Y. Wu, Z. Wu, Q. Zou, Y. Zheng, L. Zeng, T. Zhu, M. Hu, and Y. Zhang, "High N_2O_5 Concentrations Observed in Urban Beijing: Implications of a Large Nitrate Formation Pathway," Environ. Sci. Technol. Lett. **4**(10), 416–420 (2017).
35. Y. J. Tham, Z. Wang, Q. Li, H. Yun, W. Wang, X. Wang, L. Xue, K. Lu, N. Ma, B. Bohn, X. Li, S. Kecorius, J. Größ, M. Shao, A. Wiedensohler, Y. Zhang, and T. Wang, "Significant concentrations of nitryl chloride sustained in the morning: investigations of the causes and impacts on ozone production in a polluted region of northern China," Atmos. Chem. Phys. **16**(23), 14959–14977 (2016).
36. Z. Li, R. Hu, P. Xie, H. Wang, K. Lu, and D. Wang, "Intercomparison of in situ CRDS and CEAS for measurements of atmospheric N_2O_5in Beijing, China," Sci. Total Environ. **613-614**, 131–139 (2018).
37. J. M. Langridge, S. M. Ball, A. J. L. Shillings, and R. L. Jones, "A broadband absorption spectrometer using light emitting diodes for ultrasensitive, in situ trace gas detection," Rev. Sci. Instrum. **79**(12), 123110 (2008).
38. O. J. Kennedy, B. Ouyang, J. M. Langridge, M. J. S. Daniels, S. Bauguitte, R. Freshwater, M. W. McLeod, C. Ironmonger, J. Sendall, O. Norris, R. Nightingale, S. M. Ball, and R. L. Jones, "An aircraft based three channel broadband cavity enhanced absorption spectrometer for simultaneous measurements of NO_3, N_2O_5 and NO_2," Atmos. Meas. Tech. **4**(9), 1759–1776 (2011).
39. G. Schuster, I. Labazan, and J. N. Crowley, "A cavity ring down/cavity enhanced absorption device for measurement of ambient NO_3 and N_2O_5," Atmos. Meas. Tech. **2**(1), 1–13 (2009).
40. S. S. Brown, H. Stark, S. J. Ciciora, R. J. McLaughlin, and A. R. Ravishankara, "Simultaneous in situ detection of atmospheric NO_3 and N_2O_5 via cavity ring-down spectroscopy," Rev. Sci. Instrum. **73**(9), 3291–3301 (2002).
41. W. P. Dubé, S. S. Brown, H. D. Osthoff, M. R. Nunley, S. J. Ciciora, M. W. Paris, R. J. McLaughlin, and A. R. Ravishankara, "Aircraft instrument for simultaneous, in situ measurement of NO_3 and N_2O_5 via pulsed cavity ring-down spectroscopy," Rev. Sci. Instrum. **77**(3), 034101 (2006).
42. H. Fuchs, W. P. Dubé, S. J. Ciciora, and S. S. Brown, "Determination of inlet transmission and conversion efficiencies for in situ measurements of the nocturnal nitrogen oxides, NO_3, N_2O_5 and NO_2, via pulsed cavity ring-down spectroscopy," Anal. Chem. **80**(15), 6010–6017 (2008).
43. N. L. Wagner, W. P. Dube, R. A. Washenfelder, C. J. Young, I. B. Pollack, T. B. Ryerson, and S. S. Brown, "Diode laser-based cavity ring-down instrument for NO_3, N_2O_5, NO, NO_2 and O_3 from aircraft," Atmos. Meas. Tech. **4**(6), 1227–1240 (2011).
44. C. A. Odame-Ankrah and H. D. Osthoff, "A compact diode laser cavity ring-down spectrometer for atmospheric measurements of NO_3 and N_2O_5 with automated zeroing and calibration," Appl. Spectrosc. **65**(11), 1260–1268 (2011).
45. R. Hu, D. Wang, P. Xie, M. Qin, C. Li, and J. Liu, "Diode laser cavity ring-down spectroscopy for atmospheric NO_3 radical measurement," Wuli Xuebao **63**(11), 110707 (2014).
46. E. C. Wood, P. J. Wooldridge, J. H. Freese, T. Albrecht, and R. C. Cohen, "Prototype for in situ detection of atmospheric NO_3 and N_2O_5 via laser-induced fluorescence," Environ. Sci. Technol. **37**(24), 5732–5738 (2003).
47. J. Matsumoto, H. Imai, N. Kosugi, and Y. Kajii, "In situ measurement of N_2O_5 in the urban atmosphere by thermal decomposition/laser-induced fluorescence technique," Atmos. Environ. **39**(36), 6802–6811 (2005).

Optics EXPRESS

48. X. Wang, T. Wang, C. Yan, Y. J. Tham, L. Xue, Z. Xu, and Q. Zha, "Large daytime signals of N_2O_5 and NO_3 inferred at 62 amu in a TD-CIMS: chemical interference or a real atmospheric phenomenon?" Atmos. Meas. Tech. **7**(1), 1–12 (2014).
49. D. L. Slusher, L. G. Huey, D. J. Tanner, F. M. Flocke, and J. M. Roberts, "A thermal dissociation–chemical ionization mass spectrometry (TD-CIMS) technique for the simultaneous measurement of peroxyacyl nitrates and dinitrogen pentoxide," J. Geophys. Res. **109**(D19), D19315 (2004).
50. J. P. Kercher, T. P. Riedel, and J. A. Thornton, "Chlorine activation by N_2O_5: simultaneous, in situ detection of $ClNO_2$ and N_2O_5 by chemical ionization mass spectrometry," Atmos. Meas. Tech. **2**(1), 193–204 (2009).
51. O. Abida, L. H. Mielke, and H. D. Osthoff, "Observation of gas-phase peroxynitrous and peroxynitric acid during the photolysis of nitrate in acidified frozen solutions," Chem. Phys. Lett. **511**(4–6), 187–192 (2011).
52. H. Yi, T. Wu, A. Lauraguais, V. Semenov, C. Coeur, A. Cassez, E. Fertein, X. Gao, and W. Chen, "High-accuracy and high-sensitivity spectroscopic measurement of dinitrogen pentoxide (N_2O_5) in an atmospheric simulation chamber using a quantum cascade laser," Analyst (Lond.) **142**(24), 4638–4646 (2017).
53. D. Wang, R. Z. Hu, P. H. Xie, J. G. Liu, W. Q. Liu, M. Qin, L. Y. Ling, Y. Zeng, H. Chen, X. B. Xing, G. L. Zhu, J. Wu, J. Duan, X. Lu, and L. L. Shen, "Diode laser cavity ring-down spectroscopy for in situ measurement of NO_3 radical in ambient air," J. Quant. Spectrosc. Radiat. Transf. **166**, 23–29 (2015).
54. A. O'Keefe and D. A. G. Deacon, "Cavity ring-down optical spectrometer for absorption-measurements using pulsed laser sources," Rev. Sci. Instrum. **59**(12), 2544–2551 (1988).
55. R. Atkinson and J. Arey, "Atmospheric Degradation of Volatile Organic Compounds," Chem. Rev. **103**(12), 4605–4638 (2003).
56. G. Berden, R. Peeters, and G. Meijer, "Cavity ring-down spectroscopy: Experimental schemes and applications," Int. Rev. Phys. Chem. **19**(4), 565–607 (2000).
57. R. Hu, D. Wang, P. Xie, H. Chen, and L. Ling, "Diode Laser Cavity Ring-Down Spectroscopy for Atmospheric NO_2 Measurement," Acta Opt. Sin. **36**(2), 0230006 (2016).
58. H. Fuchs, W. R. Simpson, R. L. Apodaca, T. Brauers, R. C. Cohen, J. N. Crowley, H. P. Dorn, W. P. Dubé, J. L. Fry, R. Haseler, Y. Kajii, A. K. -Scharr, I. Labazan, J. Matsumoto, T. F. Mentel, Y. Nakashima, F. Rohrer, A. W. Rollins, G. Schuster, R. Tillmann, A. Wahner, P. J. Wooldridge, and S. S. Brown, "Comparison of N_2O_5 mixing ratios during NO3Comp 2007 in SAPHIR," Atmos. Meas. Tech. **5**(11), 2763–2777 (2012).
59. G. J. Phillips, J. Thieser, M. Tang, N. Sobanski, G. Schuster, J. Fachinger, F. Drewnick, S. Borrmann, H. Bingemer, J. Lelieveld, and J. N. Crowley, "Estimating N_2O_5 uptake coefficients using ambient measurements of NO_3, N_2O_5, $ClNO_2$ and particle-phase nitrate," Atmos. Chem. Phys. **16**(20), 13231–13249 (2016).
60. R. Atkinson, D. L. Baulch, R. A. Cox, J. N. Crowley, R. F. Hampson, R. G. Hynes, M. E. Jenkin, J. A. Kerr, M. J. Rossi, and J. Troe, "IUPAC Subcommittee for gas kinetic data evaluation," Evaluated kinetic data. *http://www.iupac-kinetic.ch.cam.ac.uk/*.
61. S. Voigt, J. Orphal, and J. P. Burrows, "The temperature and pressure dependence of the absorption cross-sections of NO_2 in the 250–800 nm region measured by Fourier-transform spectroscopy," J. Photochem. Photobiol. **149**(1–3), 1–7 (2002).
62. J. B. Burkholder and R. K. Talukdar, "Temperature dependence of the ozone absorption spectrum over the wavelength range 410 to 760 nm," Geophys. Res. Lett. **21**(7), 581–584 (1994).
63. P.-F. Coheura, S. Fallya, M. Carleera, C. Clerbauxa, R. Colina, A. Jenouvrierb, M.-F. Merienneb, C. Hermansc, A. C. Vandaelec, "New water vapor line parameters in the 26000–13000 cm^{-1} region," J. Quant. Spectrosc. Radiat. Transf. **74**, 493–510 (2002).
64. P. Zalicki and R. N. Zare, "Cavity ring-down spectroscopy for quantitative absorption-measurements," J. Chem. Phys. **102**(7), 2708–2717 (1995).
65. H. D. Osthoff, M. J. Pilling, A. R. Ravishankara, and S. S. Brown, "Temperature dependence of the NO_3 absorption cross-section above 298 K and determination of the equilibrium constant for $NO_3 + NO_2 <-> N_2O_5$ at atmospherically relevant conditions," Phys. Chem. Chem. Phys. **9**(43), 5785–5793 (2007).
66. R. J. Yokelson, J. B. Burkholder, R. W. Fox, R. K. Talukdar, and A. R. Ravishankara, "Temprature dependence of the NO_3 absorption-spectrum," J. Phys. Chem. **98**(50), 13144–13150 (1994).
67. D. Asaf, D. Pedersen, V. Matveev, M. Peleg, C. Kern, J. Zingler, U. Platt, and M. Luria, "Long-Term Measurements of NO_3 Radical at a Semiarid Urban Site: 1. Extreme Concentration Events and Their Oxidation Capacity," Environ. Sci. Technol. **43**(24), 9117–9123 (2009).
68. R. A. Washenfelder, N. L. Wagner, W. P. Dubé, and S. S. Brown, "Measurement of Atmospheric Ozone by Cavity Ring-down Spectroscopy," Environ. Sci. Technol. **45**(7), 2938–2944 (2011).

1. Introduction

Nitrate radical (NO_3) and dinitrogen pentoxide (N_2O_5) are interesting trace gas constituents of the troposphere, which play an important role in nocturnal chemical processes. The NO_3 radical is a major oxidant for pollutants, including a number of volatile organic compounds (VOCs) that are important for photochemical ozone production during the night and for controlling the lifetime of some species [1, 2]. N_2O_5, the heterogeneous loss of which can affect the oxidant ability of NO_3 [3], is the reservoir specie of the NO_3 radical. At night, NO_x

Optics EXPRESS

is removed from the troposphere mostly via reactions with NO_3 and heterogeneous hydrolysis of N_2O_5 [3–5]. In addition, The heterogeneous reactions of N_2O_5 and NO_3 also play a vital role in the generation of aerosol nitrate, as well as in the aging of secondary organic aerosols [6]. Furthermore, the presence of N_2O_5 in the troposphere enables halogen activation, forming $ClNO_2$, which can photolyze during the day and yield a highly reactive chlorine radical and NO_2. All of these processes can directly and indirectly have an impact on climate. NO_3 is produced from oxidation of NO_2 by ozone (O_3) [Eq. (1)] and rapidly equilibrates with NO_2 and N_2O_5 [Eq. (2)] in ambient air. The equilibrium partitioning between NO_3 and N_2O_5 is determined by NO_2 concentration and ambient temperature [7]. N_2O_5 is favored by high NO_2 concentrations and low temperatures.

$$NO_2+O_3 \rightarrow NO_3+O_2 \quad (1)$$

$$NO_3+NO_2+M \leftrightarrow N_2O_5+M \quad (2)$$

NO_3 is short-lived in sunlit air due to its strong absorption and photolysis by visible light [Eq. (3) and Eq. (4)] as well as its reactivity towards NO [8] (Eq. (5)), a predominantly daytime species. In general, NO_3 is negligible in the daytime; however, under some specific conditions, such as coexistence of high ozone and NO_2, high aerosol scattering coefficient and weak solar irradiation, NO_3 and its reservoir N_2O_5 have been inferred as significant oxidants in the process of the formation of ozone and secondary aerosols [9–11].

$$NO_3+h\upsilon \rightarrow NO+O(90\%) \quad (3)$$

$$NO_3+h\upsilon \rightarrow NO+O_2(10\%) \quad (4)$$

$$NO_3+NO \rightarrow 2NO_2 \quad (5)$$

The NO_3 radical reacts rapidly with various VOCs [12] to produce nitric acid and a hydrocarbon radical [Eq. (6)]. The reactions of the NO_3 radical with biogenic hydrocarbons such as isoprene and monoterpenes may be a vital mechanism for the production of secondary organic aerosol [13–15]. N_2O_5 is lost mainly by heterogeneous hydrolysis on aerosol surfaces to produce nitrate [Eq. (7)] or by the reaction between N_2O_5 and H_2O to generate nitric acid [2, 16, 17] [Eq. (8)].

$$NO_3+VOC \rightarrow \text{products} \quad (6)$$

$$N_2O_5+\text{aerosol} \rightarrow \text{nitrate} \quad (7)$$

$$N_2O_5+H_2O \rightarrow 2HNO_3 \quad (8)$$

Given the importance of the NO_3 radical and N_2O_5 in the nocturnal chemical process, in the past dacades, a wide range of surface-based field studies have been conducted to investigate the nighttime chemistry of NO_3 and N_2O_5 in polluted and clean air environments [11, 16–24]. Also, more limited measurements have been made on other platforms, such as aircrafts [14, 25, 26], towers [27, 28] and ships [4]. Moreover, only a small amount of existing research on NO_3 and N_2O_5 can be used to analyzer the vertical profiles of NO_3 and N_2O_5 [29–31]. The simultaneous measurement of NO_3 and N_2O_5 remains an area of considerable interest. Particularly, in densely populated urban areas, the ground-based measurements of NO_3 and N_2O_5 have become more difficult because of local emissions. Thus, it is of great importance to investigate the vertical gradients of NO_3 and N_2O_5 and access the influence of significant sinks of these species in urban area. Particularly, in China, home to several megacities and many large cities owing to its fast-paced urbanizations and industrialization processes, only a few measurements have been reported to investigate the role of NO_3 and N_2O_5 in the atmosphere [11, 32–36],so field measurements should be

Optics EXPRESS

conducted in these regions to obtain a full picture of the role of the NO_3 oxidation process and N_2O_5 heterogeneous reactions in the formation of aerosol in China.

With the aim of obtaining a detailed understanding of the chemistry involving NO_3 and N_2O_5, the simultaneous measurement of NO_3 and/or N_2O_5 have been performed by several groups using cavity enhanced absorption spectroscopy (CEAS) [32, 37–39], cavity ring-down spectroscopy (CRDS) [21, 40–45], laser induced fluorescence [46, 47] and chemical ionization mass spectrometry (CIMS) [48–50]. With respect to CIMS which combines the ion-molecule chemistry with mass spectrometry detection, fundamental measurement involves the reaction of I^- (the reagent ion) with NO_3 to form the NO_3^- ion that can be detected at 62 amu. However, this method may suffer interference, such as N_2O_5, HNO_3 and HO_2NO_2 [48, 49, 51].CIMS method based on iodide cluster ion at m/z 235 has been successfully used in N_2O_5 measurement [50]. With respect to the optical methods, the measurement of NO_3 is based on the strong absorption of NO_3 in the visible spectrum at 662 nm whereas the measurement of N_2O_5 is determined by using a heated channel to decompose it into NO_3 or from the calculation according to the fast equilibrium among N_2O_5, NO_3 and NO_2. The thermal dissociation system of LIF is similar to that of CRDS for N_2O_5 detection, but for the fomer NO_3 is measured by LIF technique. The LIF technique has achieved a detection limit of 8 and 11 pptv for NO_3 and N_2O_5 with an intergration time of 10 min, respectively [47]. However, due to the relatively low fluorescence quantum yield of NO_3, this method has not been widely used. The CEAS and CRDS techniques are two similar optical techniques. The ringdown signal of a light pulse circulating inside a ringdown cavity both depends on the reflectivity of the mirrors and the attenuation by gases and aerosol particles present in the cavity. But CRDS monitors the absorption information at the peak absorbtion wavelength while CEAS requires obtaining the obsorber's absorption data over a wide wavelength. The reported NO_3 and N_2O_5 detection sensitivities for CEAS and CRDS achieve similar detection performance ranging from 0.5 pptv–8 pptv with a high temporal resolution of a few seconds. The high-speed measurements and universal detection capabilities are advantageous since the instrument can rapidly respond to concentration changes. CEAS and CRDS can achieve background measurement by adding excess NO to titrate NO_3 and N_2O_5. However, the advantage of NO_3 removal for those two methods comes at the expense of potential wall losses, which have to be characterized. In recent years, a spectroscopic instrument based on a mid-infrared external cavity quantum cascade laser (EC-QCL) was developed to measure N_2O_5 directly based on the N_2O_5 strong absorption bands in the mid-infrared region centered approximately at 1,245 cm^{-1} [52]. The minimum detection limit was 15 ppbv with an integration time of 25 s and it was down to 3 ppbv in 400 s with an optical absorption path-length of Leff = 70 m. This method has just been used in a chamber experiment, not in the field environments.

Based on the current research development on NO_3 and N_2O_5 in China, the following two requirements have been proposed for the instruments. First, instruments should have a high time resolution and a high detection limit to capture the rapid change of NO_3 and N_2O_5, such as in a ground site where many local source emissions exist. Second, instruments should have a compact structure to apply to the vertical profile measurement, such as on a movable carriage. Here, we report a two channel CRDS system for the detection of NO_3 and N_2O_5. Previous CRDS instruments used by our group for the detection of NO_3 have been described [53] and successfully deployed in ground sites. Major modifications to the device include the introduction of a second cavity to enable the simultaneous measurement of NO_3 and N_2O_5 and the optimization of operating parameters i.e., flow rates and residence time as well as the improvement of detection limit and time resolution. The instrument we describe here is able to detect pptv levels of NO_3 and N_2O_5 on timescales of a few seconds in a well defined air-mass (point measurement). In addition, the instrument has a small footprint of 110 × 40 × 35 cm, low power consumption of < 300W and a total weight of < 40 kg, such that it can be

Optics EXPRESS

widely used in different platforms. The instrument was deployed to detect the mixing ratios of NO_3 and N_2O_5 in the urban city of Beijing in summer and winter campagains.

2. Experimental

2.1 Cavity ring-down spectroscopy

CRDS, first demonstrated in 1988 [54] is a scheme for highly sensitive absorption measurements and has been described in several reviews [55–57] and we present it briefly to clarify the notation used in this study. Laser is coupled into a high finesse optical cavity. The leaked intensity from the back of a highly reflective mirror, I(t), exhibits as a single exponential decay with a time constant, τ_0, that is inversely proportional to the mirror transmission. The concertration of the target absorber can be accomplished by comparing the fitted ring-down time constants in the presence (τ) and absence of the absorber (τ_0) using the absorption cross section (σ) at the probing wavelength.

$$[A]=\frac{R_L}{c\sigma}\left(\frac{1}{\tau}-\frac{1}{\tau_0}\right) \tag{9}$$

where, c is the speed of the light, R_L is the ratio of the total cavity length to the length over which the absorber is present in the cavity and τ and τ_0 are ring-down time constants in the presence (τ) and absence (τ_0) of the absorber respectively.

2.2 Optical layout

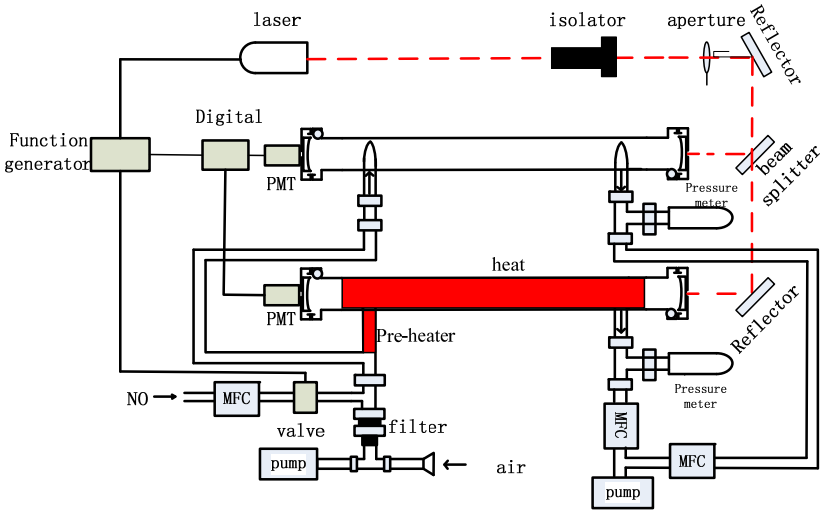

Fig. 1. A schematic of the two channel CRDS instrument for the detection of NO_3 and N_2O_5.

The optical layout of the two-channel CRDS instrument is described schematically in Fig. 1. Light is provided by an external modulation diode laser (IQm, Power Technology Inc.), which is pulsed through a function generator (DG1022, RIGOL), the laser output is modulated with a square-wave signal at a repetition rate of 1 KHz, which is higher than that used in Dan Wang [53], with an output power of approximately 100 mW. The laser is temperature tuned corresponding to a central wavelength of 662.08 nm. Light emerging from the laser is isolated through an optical isolator (IO-3D-660-VLP, Thorlabs) from the cavities to prevent potentially damaging back reflection from entering the laser. The light is divided into two beams by a 50/50 beam splitter and coupled into two identical 76 cm long optical cavities each constructed from pairs of high reflectivity mirrors, with reflectivities of 0.99998 and radii of curvature of 1 m. The cavity ring-down mirrors are seated in custom-built mirror

Optics EXPRESS

holders. The sample cells are constructed from PFA Teflon and are held in place by two custom-built aluminum enclosures. NO_3 is detected via its strong $\tilde{B}^2E'(0000) \leftarrow \tilde{X}^2A_2'(0000)$ electronic transition centered at approximately 662 nm. N_2O_5 is measured in another cavity maintained at 80 °C following its thermal coversion to NO_3 and NO_2 at 140 °C in a heater placed before the cavity entrance. Therefore the sum of ambient NO_3 and thermally dissociated N_2O_5 is measured in this channel. The temperature of the two stage heated channel is close to that of the NOAA-CRDS instrument where ambient air initially flows through a Teflon converter maintained at 140 °C and subsequently into the measurement cell maintained at 80 °C [58]. The preheater temperature is determined using tape heaters wrapped around a 35 cm-long, 1/4 o.d. and 3/16 i.d. section of Teflon tubing with embedded pt100 thermocouples and temperature controllers (Yudian-Ai509). The time needed for quantitative conversion is mainly limited by the time needed to heat the sampled air. Calculations using a value of k2b = 23.4 s^{-1} at 80 °C and 1 atm [59] for N_2O_5 indicate that less than 0.1 s N_2O_5 is stoichiometrically converted to NO_3. The specific design of the heater enables the gas to convert to NO_3 completely with the gas residence time of 0.10 s in the tube when the flow rate is 3.5 slm. Each mirror is isolated from the sample flow by a purge volume that is continuously flushed with 100-200 sccm of dry nitrogen to prevent the degradation of reflectivity by aerosols to mirror surfaces during the night. Light exiting the back mirror of the cavity is monitored by a photomultiplier tubes (PMT, Hamamatsu H10721-20) after passing through a 660 nm band pass filters placed in front of the PMTs to prevent stray light from unwanted wavelengths.

By digital fitting using an oscilloscope card (PCI 6132, 2.5 MHz) at a rate of 1.0×10^6 samples s^{-1} per channel, the 2,000 ring-down traces are transferred to a computer, co-added and averaged on the occasion when data are acquired on the data acquisition board for a continuous period of 2.5 s. This data acquisition method, which was the same as that used by osthoff [43], can both improve the fitting rate compared with finite sampling and avoid data loss compared with continuous sampling. The LM fitting method is used to obtain the average of the ring-down traces. The effective absorbtion optical path excees 30 km, with the fitting ringdown-time of approximately 100 μs (τ_0), which is sufficient for NO_3 radical and N_2O_5 measurements. An example cavity decay trace is shown in Fig. 2.

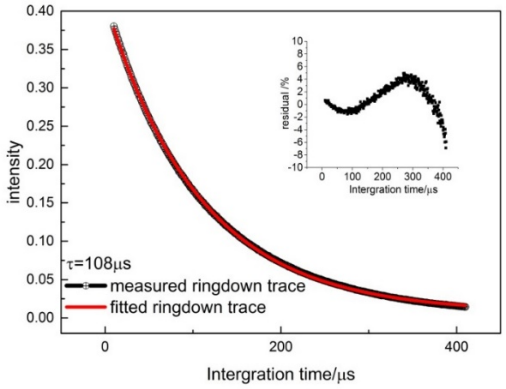

Fig. 2. An example of cavity ring-down signal and the fitting result. The lower panel is the fitting residual trace.

The inlet consists of several parts. First sample air is brought into the instrument enclosure by a short length of 0.4 cm inner diameter tubing. The sample air passes through a 47 mm-diameter, 2μm-pore size, 25 μm-thick Teflon filter to remove all optically active

Optics EXPRESS

particles from the sample air flow. The filter is usually changed every one or two hours beacause of aging effects, although changes occur more frequently in heavily polluted environment. A T-piece PFA Teflon connector was used to connect the two sample channels. The slow flow system is separated into two air samples immediately below the filter each of which is controlled by electronic mass flow controllers at the exhaust. A pump with a capacity of 11 L is applied to both flows. Flow rates are usually 5 slm and 3.5 slm for the ambient temperature channel and the two-stage heated channel, respectively.

The ring-down time of the absorber in the absence of the cavity is determined by the titration reaction of NO with NO_3 [Eq. (6)] [19, 21, 40]. NO (10 ppm) is added at a flow rate of 50 sccm through an MFC to the air after the filter every 300 s for a period of 60s. The added NO is about 1.4×10^{12} molecule/cm^3 at a total flow of 8.5 slm. The rate constant of Eq. (5) is 2.6×10^{-11} cm^3 molecule^{-1} s^{-1} at 298 K and is weakly dependent on temperature. Based on the evaluated rate coefficient [60], this amount of NO should result in complete titration of NO_3 within 0.1 s. This process disturbs the equilibrium between NO_3 and N_2O_5, and leads to NO_3 formation by N_2O_5 dissociation, such that the NO added titrates all NO_3 and N_2O_5. When NO is added, NO_3 is converted into NO_2 in its reaction with NO before entering the cavity, so that the NO_3 absorption can be selectively switched on and off. The data obtained for the first 30 s period after adding NO are excluded from the data collection, taking the residence time into account. The largest uncertainty of the NO_3 radical caused by the background shift during the 5 min period is approximately ± 0.5 pptv (the variations of O_3, NO_2 and H_2O are estimated at ± 2 ppbv, ± 2 ppbv and ± 2%, respectively).

The data also should be corrected due to the loss of NO_3 and N_2O_5 during transport through the cavities. Because the ambient N_2O_5 concentration is determined from the two measured results in ambient channel and heated channel, the NO_3 transmission efficiency in ambient channel (Te(NO_3)amb) and the NO_3 + N_2O_5 transmission efficiency (Te(N_2O_5)) in heated channel have to be known to accurately retrieve the ambient concentration of NO_3 and N_2O_5.

In the case of NO_3 in ambient channel, the loss should include the wall loss in the sampling tube and the detection cell as well as the loss in the filter and filter holder. The NO_3 wall loss has been measured by flowing a stable NO_3 source into the cavity as described previously [53], the linear fit of NO_3 concentration with the residence time results in a NO_3 first order loss rate coefficient and associated uncertainty of k = 0.19 ± 0.02 s^{-1},which is in good agreement with that measured by Dube et al. [41] (0.20 ± 0.05 s^{-1}). The residence time through the inlet tube to the midpoint of the ring-down cell is 0.74 s when the flow rate is 5 slm, so that the NO_3 wall loss is 14% ± 1%. The loss in the filter holder and filter has been measured by repeated flowing NO_3 (generated in the reaction of NO_2 with O_3) into the cavities with the insertion and removal of a filter holder and a filter. The results show that the loss in a filter holder and a clean filter is 17 ± 5% while the loss increased by 2% in a used filter and filter holder. During the campaign, the filter is changed every 0.5 - 2 h depending on the aerosol loadings. For example, under heavy polluted conditions (PM2.5 > 200 μg/m^3), the filter is changed every 0.5 h to reduce the impact of the filter aging on the measurement. Overall, the NO_3 transmission efficiency (Te$(NO_3)_{amb}$) is 69% ± 5%.

For the determination of the N_2O_5 + NO_3 transmission efficiency in the heated channel, the N_2O_5 loss in the filter and the inlet tube before the sampled air flows into the pre-heater as well as the wall loss of NO_3 in the pre-heater and the detection cavity should be taken into account while the loss of NO_3 in the filter can be neglected due to the large ratio of N_2O_5/NO_3. Such as under the conditions of 10 °C and NO_2 of 20 ppbv, the ratio of N_2O_5/NO_3 is larger than 100. Since N_2O_5 itself has a little filter and inlet loss of 2% before flowing into the preheating tube which is minor compared to NO_3 as described previously [23, 41], the only significant contribution to the N_2O_5 sampling efficiency is the wall loss occurring subsequent to its conversion to NO_3 downstream of the heater. The surface materials of the preheating tube and the detection cavity in the heated channel are the same as that in the

ambient channel. Therefore, the wall loss reactivity of NO_3 in the ambient will be applicable for the converted NO_3 in the heated channel. The residence time through the heated sections of the flow system to the midpoint of the ring-down cell is 0.63 s, so that the NO_3 in the heated portion of the inlet is 12 ± 2%. The correction transmission factor for the measurement of N_2O_5 + NO_3 was thus determined as 86% ± 2%.

3. Results

3.1 Selection of laser diode and effective absorption cross-section

The diode output is centered at 662.08 nm (as shown in Fig. 3 red lines), lightly to the red of the NO_3 absorption maximum. In selecting the centered wavelength, the interference of other trace gases such as NO_2 [61], O_3 [62] and H_2O [63], whose absorption cross sections are shown in Fig. 3, and the full width at half maximum of the diode laser, which should be significantly smaller than that of the NO_3 radical absorption width, have been considered to ensure the single exponential decay of the measured ring-down signal of the NO_3 radical [64]. To retrieve molecule number densities from the Eq. (7) and Eq. (8), the effective absorption cross section of the ambient absorbers in ambient and hot temperature is necessary in this wavelength. The NO_3 absorption cross section is known to be temperature dependent [65, 66]. By convolution of the laser spectrum and the absorption cross section of the NO_3 radical [67], the NO_3 radical effective absorption cross section is 2.24×10^{-17} cm^2 $molecule^{-1}$ for our instrument in ambient temperature (the pink line in Fig. 3). The temperature dependence of the NO_3 cross section was taken from Osthoff et al. [65] and the absolute values were taken from Yokelson et al. [66] and plotted in Fig. 3 as the blue line. The value of effective absorption cross section of NO_3 at 662.08 nm is scaled to 1.80×10^{-17} cm^2 $molecule^{-1}$ at 80 °C from 2.24×10^{-17} cm^2 $molecule^{-1}$ at 25 °C.

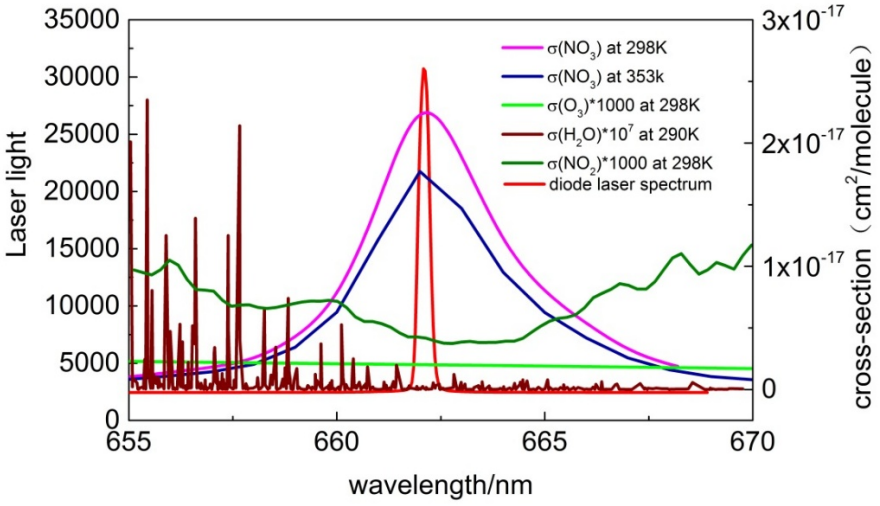

Fig. 3. Effective absorption cross section of NO_3 radical at 298K and 353K, cross section of NO_2, O_3, H_2O and diode laser spectrum.

3.2 Determination of R_L

Due to the influence of the purge volumes, the ratio of the absorption path length and the mirror distance cannot be simply derived from the actual distance between the inlet and outlet of the sampled gas and the distance between the mirrors. R_L is calibrated regularly by filling the cavity with several different known O_3 concentrations and calculating the slope of

Optics EXPRESS

the measured optical extinction vs. O_3 as described by Washenfelder [68]. O_3 is generated by passing a stream of O_2 past a 185 nm Hg lamp and the concentration is detected by an O_3 analyzer. The R_L value is 1.20. The fitted slopes were similar for all channels with an uncertainty of 5% which can be attribute to the O_3 analyzer (3%) and the absorption cross section (4%).

3.3 Calculation of the mixing ratios

Once the transmission efficiency of NO_3 in the ambient channel and the transmission efficiency of NO_3 and N_2O_5 in the heated channel are known, the number densities of NO_3 and N_2O_5 can be calculated using the following equations:

$$[NO_3]_{amb} = \frac{R_L}{Te(NO_3)_{amb} c\sigma_{ambient}} \left(\frac{1}{\tau_{ambient}} - \frac{1}{\tau_{0,ambient}}\right) \tag{10}$$

$$[N_2O_5]_{amb} = \frac{\frac{R_L}{c\sigma_{hot}}\left(\frac{1}{\tau_{hot}} - \frac{1}{\tau_{0,hot}}\right)}{Te(N_2O_5)} - [NO_3]_{amb} \tag{11}$$

where $\tau_{ambient}$ and τ_{hot} are the ring-down time constants observed in the ambient and heated channels, respectively; $\sigma_{ambient}$ and σ_{hot} are the temperature-dependent absorption cross sections of NO_3 at the absorption maximum at 662 nm; $\tau_{0,\,ambient}$ and $\tau_{0,\,hot}$ are the ring-down time constants when excess NO was added to the inlet; $Te(N_2O_5)$ is the transmission efficiency of N_2O_5 through the heated channels; and $Te(NO_3)_{amb}$ is the transmission efficiency of NO_3 through the ambient channel.

The calculated N_2O_5 mixing ratio above is based on the fact that N_2O_5 has been completely converted to NO_3. In fact, under the conditions when NO_2 concentration is less than 30 ppbv and the cavity temperature is higher than 75 °C, the conversion of N_2O_5 to NO_3 goes fully to its equilibrium value. However, under high NO_2 concentration, the fraction of N_2O_5 that remains undissociated at equilibrium at temperature of 75 °C is large (Fig. 4). The undissociated N_2O_5 is dependent on NO_2 and temperature in the cavity. The NO_2-dependent correction value ranges from 99% to 86% for NO_2 from 0 ppbv to 40 ppbv for the measured N_2O_5. Correction is particularly important in winter because of the high NO_2 concentration and low temperature. For example, in wintertime, when cavity temperature is 75°C and NO_2 is 40 ppbv, the N_2O_5 decomposition rate in the cavity is approximately 86% and the actual N_2O_5 concentration should be obtained by dividing the derived N_2O_5 data based on the equations mentioned above by this decomposition rate. Thus, a higher cavity temperature is used under such conditions, e.g., 85 °C to improve the N_2O_5 dissociation rate. Under the same conditions previously described, the decomposition rate is 93%.

Optics EXPRESS

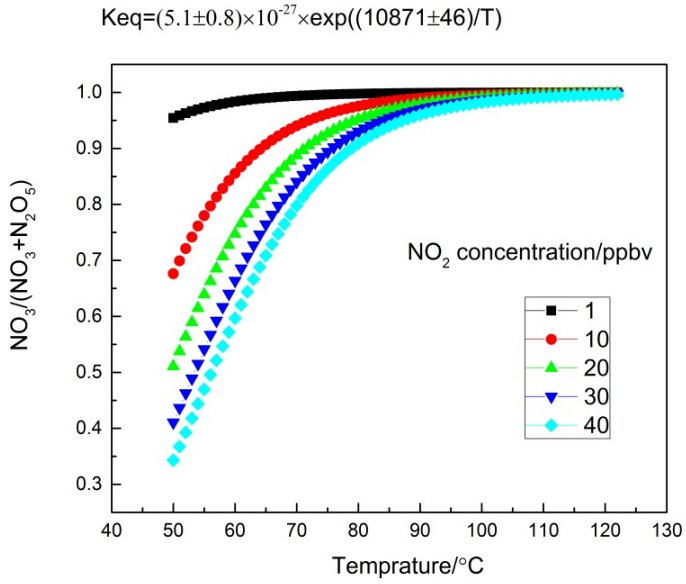

Fig. 4. The undissociated N_2O_5 ratio depend on different temperature, the different color represent different NO_2 concentration.

4. Discussion

4.1 Interference analysis

Impure NO, which contains 1×10^{10} molecule cm^{-3} level of NO_2, generates a small negative offset equivalent to 0.04 pptv NO_3 based on the fact that the NO_2 cross section in the wavelength of 662 nm is approximately 2×10^{-21} cm^2 $molecule^{-1}$, which is four orders of magnitude smaller than that of the NO_3 radical. Thus, this amount of NO_2 is too low to warrant correction. In addition, we note that adding NO to air samples containing O_3 (>20 ppbv), which also have a small absorption cross section of 1×10^{-21} cm^2 $molecule^{-1}$ at 662 nm in a typical tropospheric environment would result in the removal of O_3 and formation of NO_2 duo to its reaction with ambient O_3. The effect on the total absorption at 662 nm can be accurately applied. Taking O_3 = 100 ppbv and k (NO + O_3) = 1.9×10^{-14} cm^3 $molecule^{-1}$ s^{-1} at 298 K and an average reaction time of 0.54 s at the ambient channel, only 1.5 ppbv of O_3 is removed and 1.5 ppbv of NO_2 is generated. As a result, the overall NO_3 equivalent is 0.08 pptv. The reaction of NO with ambient O_3 to produce NO_2 is relatively slow to produce a measurable signal on the ambient channel. However, on the heated channel, taking k (NO + O_3) = 7.8×10^{-14} cm^3 $molecule^{-1}$ s^{-1} at 413 K with a reaction time of 0.10 s in the pre-heated heater and k (NO + O_3) = 4.3×10^{-14} cm^3 $molecule^{-1}$ s^{-1} at 353 K with a reaction time of 0.27 s at the center of the heated cavity, a small negative offset equivalent to 0.3 pptv NO_3 is generated. We subtract it from the ambient data set.

4.2 Optimization of signal averaging time, detection limit, and noise sources

For the red diode CRDS system, signal averaging can improve the signal-to-noise ratio. The number of average traces selected is the key issue to achieve a rapid and high sensitivity measurement. Figure 5(a) and Fig. 5(c) show a typical time series of the NO_3 and N_2O_5 instrument baselines when zero air was sampled. The Allan variance plot gives a detection limit of 2.3 pptv (1σ) for NO_3 [Fig. 5(b)] and 3.2 pptv (1σ) for N_2O_5 [Fig. 5(d)] at an interval of 2.5 s respectively. The reactor is heated to above room-temperature is carried out to

Optics EXPRESS

stabilize the dissociation of N_2O_5, which introduces strong turbulent noise because of variations in temperature in the cavity at the optimal flow rate. Thus, the detection limit of the heated channel for the detection of the sum of NO_3 and N_2O_5 is larger than that of the ambient channel for the detection of NO_3. The optimum signal averaging time is 40 s for NO_3 and 30 s for N_2O_5.

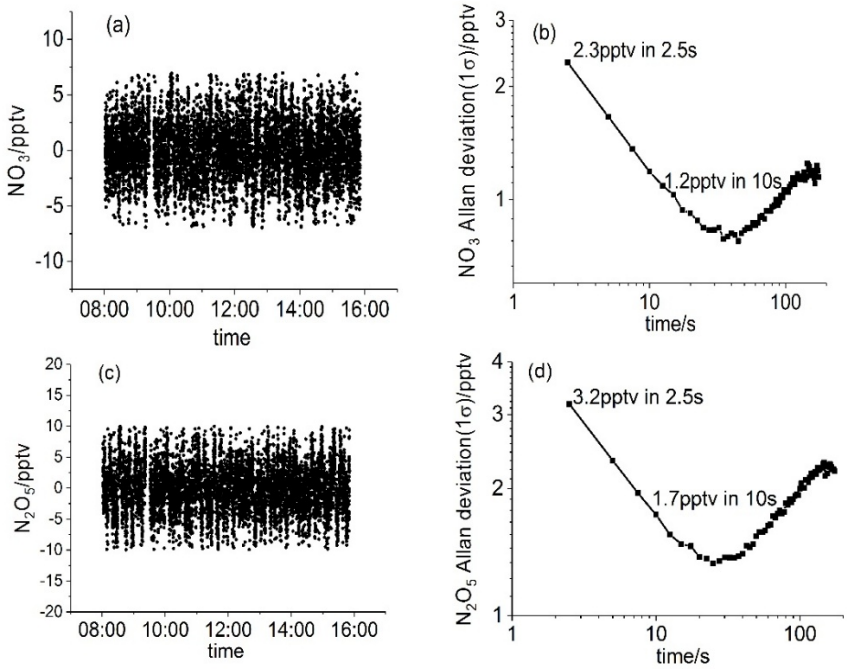

Fig. 5. Allan variance plot for the NO_3 radical measurements in ambient channel and heated channel when sampling ambient air. The instrument has 1σ precision about 2.3 pptv and 3.2 pptv in ambient channel and heated channel for a 2.5 s integration time.

The minimum detection limit of the instrument can be expressed as follows [40, 43]:

$$[X]_{min} = \frac{\sqrt{2}R_L}{c\sigma}\frac{\Delta\tau}{\tau_0^2} \quad (12)$$

where $[X]_{min}$ is the smallest measurable concentration of NO_3 and $\Delta\tau$ is the smallest measurable difference among ring-down times τ, Using RL = 1.2, τ_0 = 89.3 μs, $\sigma = 2.02 \times 10^{-17}$ cm^2 molecule^{-1} and $\Delta\tau$ = 0.16 μs for an integration time of 2.5 s in the field measurement of NO_3 in the normal channel and τ_0 = 117.4 μs, $\sigma = 1.81 \times 10^{-17}$ cm^2 molecule^{-1}, and $\Delta\tau$ = 0.35 μs for the sum of NO_3 and N_2O_5 measurement in the heated channel. The detection limits in the normal and heated channels are about 2.0 pptv (1σ) and 3.1 pptv (1σ), respectively which are consistent with the 1σ Allan variance determined from the continuous zero NO_3 and N_2O_5 measurements for the normal and heated channels.

The overall 1σ accuracy of the ambient channel is about ± 8%, as determined by the uncertainties in the absorption cross section (± 4%), path length ratio (R_L, ± 5%) and transmission efficiency (± 5%) [51]. The estimated fractional uncertainty in the quantity of the sum of ambient and dissociation NO_3 is 15%, taken as the linear sum of a 13% uncertainty in the high temperature NO_3 cross section [65], the transmission efficiency of N_2O_5 + NO_3 in the heat channel (2%) and the uncertainties of ambient NO_3 radical measurement described above (± 8%). The concentration of N_2O_5 is determined by

subtracting the ambient NO_3 measured in the ambient channel from the concentration of the sum of ambient and dissociated NO_3 measured in the heated channel. When N_2O_5 is approximate to the value of NO_3, the accuracy of NO_3 in the heated channel can significantly affect the accuracy of N_2O_5. However, when the concentration of N_2O_5 is larger than that of NO_3, the uncertainty of N_2O_5 mainly depends on the uncertainty of N_2O_5 conversion.

5. Ambient air measurements

The CRDS instrument for NO_3 and N_2O_5 measurement was deployed at the campus of Institute of Atmospheric Physics, located in urban Beijing, China (39° 58' 28″ N, 116° 22' 16″ E) to test the instrument performance. The site is surrounded by many residential and commercial areas. At 300 m east of the measurement site, there is the Jing Zang Expressway, one of the busiest main roads in the city. Influenced by mixed pollutants emitted from traffic, residential, and industrial sources, the measurement site is a good representative of urban area in Beijing.

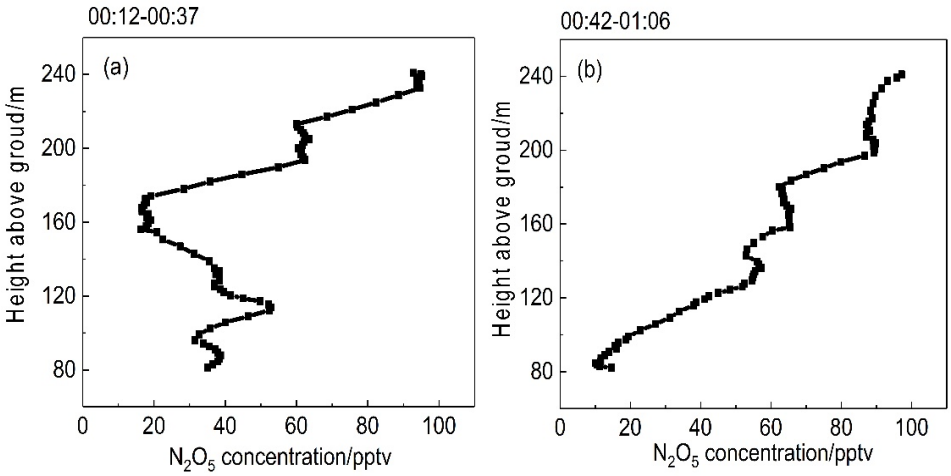

Fig. 6. N_2O_5 vertical profile at the night of 11 December, 2016. Data below 80m are not shown in the figure.

In the winter campaign, The CRDS instrument was deployed on a movable carriage and the carriage can ascend or descend the tower at a rate of about 8 m/min. The carriage can also be positioned indefinitely at an arbitrary height. During the nighttime measurement, the carriage was positioned at a height of 240 m. The carriage takes about one hour to ascend and descend once. An example of the vertical profile of N_2O_5 when the carriage was ascending and descending during 00:12 to 01:06 in 11 December is shown in Fig. 6. Data obtained at less than 80m are below the detection limit which are not shown in the figure. This finding can be attributed to local emissions such as NO. Given the cold weather and high NO_2 concentration, the thermal decomposition of N_2O_5 is relatively slow such that the N_2O_5 concentration is higher than the NO_3 concentration during the experiment. In fact, the NO_3 concentration is negligible. Results shows that the nocturnal mixing ratios of these compounds vary widely over short vertical distance scales (10 m or less). However, the N_2O_5 trend during the ascending and the descending processes within one hour is different. The N_2O_5 trend during the ascending process is complicated [Fig. 6(a)], which may be related to the different air flow disturbances. However, during the descending process [Fig. 6(b)], the N_2O_5 concentration is reduced with the carriage going down, which may be dominated by its precursors NO_2 and O_3. Overall, the results show that the instrument can be used to measure

Optics EXPRESS

the N_2O_5 vertical profile in densely populated areas and solve the difficulties in performing NO_3 and N_2O_5 measurements aloft in urban areas.

In the summer campaign, the instrument was placed in a container and the sample inlet was approximately 3 m above the ground. NO_3/N_2O_5 measurements typically started just before local sunset and stopped after the signals had returned to baseline levels following sunrise. The NO_3 and N_2O_5 time series from 2 June to 22 June, 2017 are shown in Fig. 7. In summer, due to high temperature, the chemical process involved in nighttime NO_3 radical and N_2O_5 reaction is fast. Meanwhile, influenced by vertical transmission, sudden injection of high N_2O_5 was observed, e.g. at the night of 9 June and 12 June, 2017. Thus, our instruments with high sensitivity detection have advantages in capturing these rapid chemical processes. During the entire campaign, the observed mean NO_3 and N_2O_5 mixing ratios were 36.2 pptv and 2.5 pptv, respectively. Data along with temperature and NO_2 concentration obtained by a CEAS instrument observed at nighttime of 12 June, 2017 are shown in Fig. 8. Based on Eq. (2) and taking the equilibrium constant to be Keq = (5.1 ± 0.8) × 10^{-27} × Exp((10871 ± 46)/T) cm^3/ molecule, a point-by-point comparison of the measured NO_3 mixing ratio with that calculated (green line in Fig. 9) from the NO_2 and N_2O_5 observations and the temperature was conducted. The results show that NO_3 (calculated) = NO_3 (measured) × 0.9-0.25 pptv, with a correlation coefficient R = 0.94 (Fig. 9), which can provide a confirmation of the measurement accuracy of the instruments.

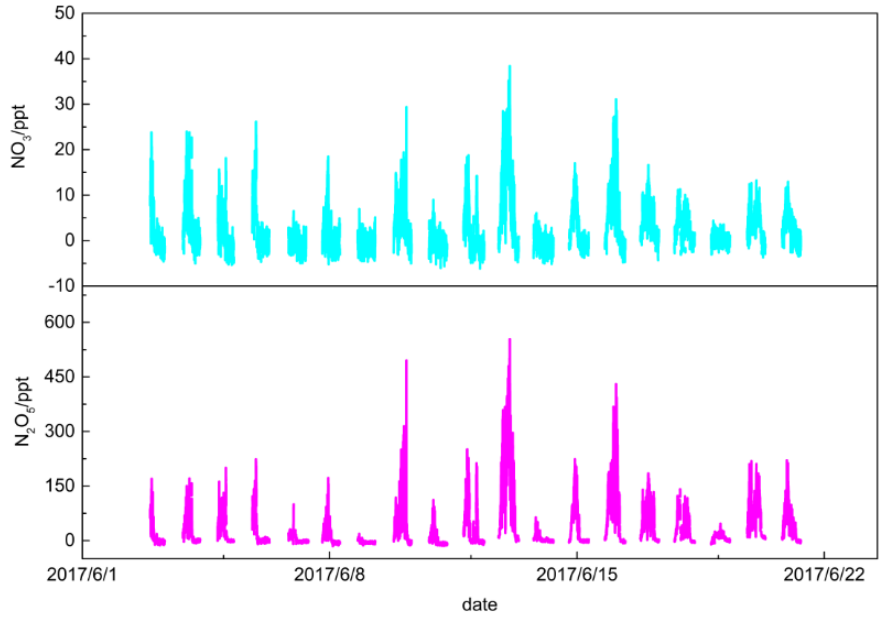

Fig. 7. NO_3 and N_2O_5 time series from 2 June to 22 June, 2017.

Optics EXPRESS

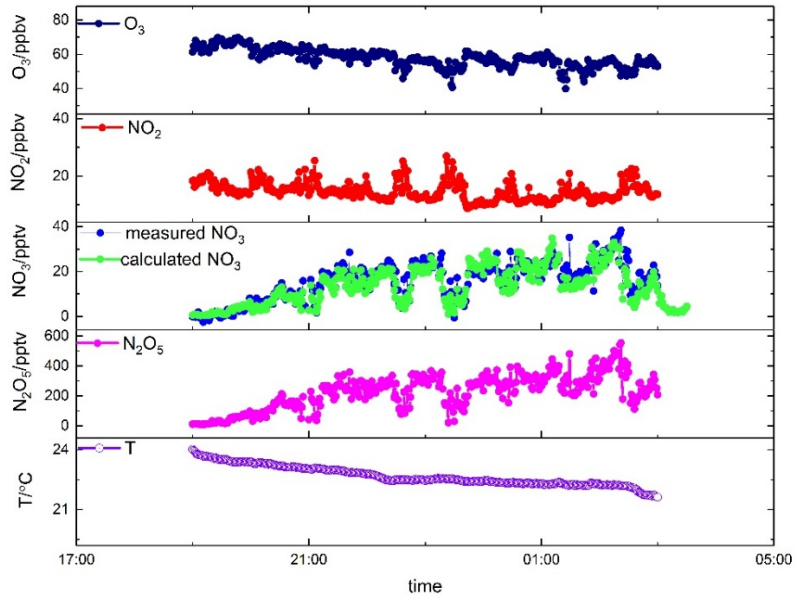

Fig. 8. O_3、NO_2、NO_3、N_2O_5 and temperature time series from 19:00 on 12 June, 2017 to 03:00 13 June, 2017. NO_3 and N_2O_5 mixing ratios are observed by the CRDS instrument. NO_2 mixing ratios are measured by a CEAS instrument. O_3 mixing ratios are measured by an ozone analyzer (Thermo Fisher 49i). All data are averaged to 1min.

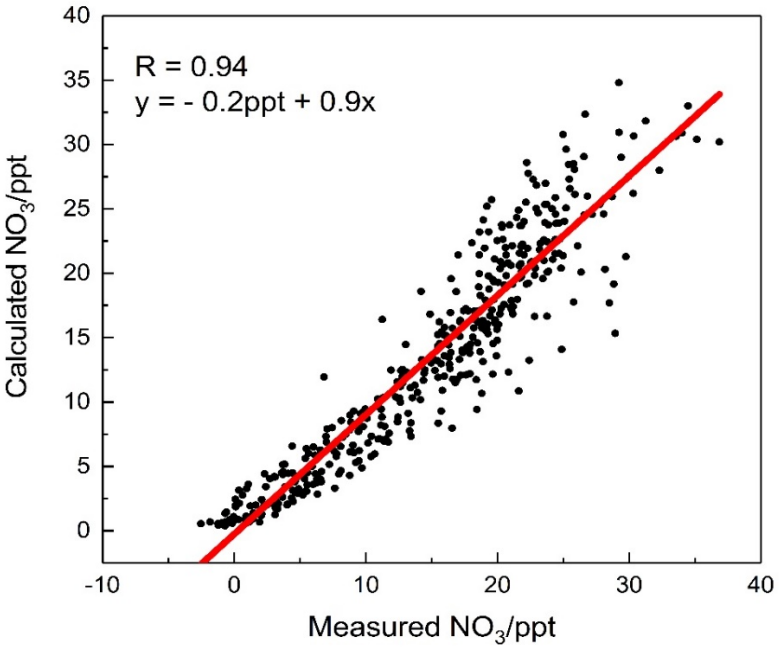

Fig. 9. Scatter plots for the calculated NO_3 from the equilibrium between NO_2 and N_2O_5 and measured NO_3. The red line illustrates the linear regression.

Optics EXPRESS

6. Conclusions and future work

The operating principles, instrumentation and field deployment of a CRDS system have been described. The instrument is able to make sensitive measurements of the concentrations of short-lived trace gases NO_3 and N_2O_5 via their absorption at 662 nm. The overall uncertainty of the instrument is 8% and 15% for NO_3 and N_2O_5 measurements, respectively. The first field deployment of the instrument was in the urban city of Beijing in December of 2016. The field observation results showed that N_2O_5 had distinct vertical concentration profiles at night in winter. To our knowledge, this study is the first time that a CRDS instrument is applied to detect N_2O_5 vertical profiles in the urban area of Beijing, China. This measurement is meaningful because it can avoid local characteristics and give an insight into turbulence processes throughout the depth of the boundary layer to some extent. Another measurement of NO_3 radical and N_2O_5 performed at nighttime of 12 June, 2017 clearly revealed the equilibrium among NO_2, NO_3 and N_2O_5. Therefore, the capability of the CRDS instrument to make rapid measurements of atmospheric trace gases and capture their spatial and temporal variability can help us understand the nighttime NO_3 chemistry on a large scale.

Funding

National Natural Science Foundation of China (41530644, 41571130023, 61575206 and 91644107); the National Key Research and Development Program of China (2017YFC0209403 and 2017YFC0209401).